Results in Physics 37 (2022) 105530

Contents lists available at ScienceDirect

Results in Physics

journal homepage: www.elsevier.com/locate/rinp

Dynamic susceptibility of a Bloch point singularity confined in a magnetic nanowire

Guidobeth Sáez [a], Eduardo Saavedra [b], Nicolás Vidal-Silva [c,*], Juan Escrig [b,d], Eugenio E. Vogel [c,d]

[a] Departamento de Física, FCFM, Universidad de Chile, Santiago, Chile
[b] Departamento de Física, Universidad de Santiago de Chile (USACH), Avda. Víctor Jara 3493, Santiago, Chile
[c] Departamento de Ciencias Físicas, Universidad de La Frontera, Casilla 54-D, 4811186 Temuco, Chile
[d] Center for the Development of the Nanoscience and Nanotechnology (CEDENNA), Avda. Víctor Jara 3493, Santiago, Chile

ARTICLE INFO

Keywords:
Bloch points
Magnetic singularity
Dynamic susceptibility
Magnetic nanowires

ABSTRACT

In this work, we have explored the dynamic properties of a Bloch Point singularity confined in a diameter-modulated magnetic nanowire. By means of micromagnetic simulations, we have characterized the system when varying the position at which the modulation is located as well as the response under a constant magnetic field. We found that the presence of the Bloch Point promotes the emergence of two distinct modes with energies above the lowest energy mode. These modes are differently affected when the geometry of the system changes and with the application of a magnetic field. However, as a general result, the Bloch Point modes are split for high magnetic fields and when the modulation is near the end of the nanowire. Thus, our results might establish a valuable strategy for detecting Bloch Point singularities.

Introduction

Cylindrical magnetic nanowires are currently at the heart of building new technologies in information processing and storage. They have been proposed as detectors of electromagnetic pulses [1], microwave circulators or phase shifters [2–5]. One of the highlighted features of magnetic nanowires is the variety of magnetic configurations that can be hosted in them, which might appear in the magnetization reversal processes or as (meta)stable states. For instance, it has been reported that according to its geometry, the system can reverse its magnetization through transverse or vortex domain walls [6,7]. Different magnetic textures can be stabilized when reducing the length of the nanostructure, converting it into a nanodisk or nanodot. In such cases, and depending on the energy contributions, magnetic vortices or skyrmions structures can emerge as insulated solitons or as cluster structures too [8–11].

A very interesting class of 3D magnetic textures appears, for instance, at the core of a vortex domain wall, the so-called Bloch Points (BPs) [12–20]. A BP can be defined as a magnetic singularity that usually leads to the transition between distinct magnetic configurations. For instance, it has been shown that the annihilation of skyrmions confined to nanodots is mediated by the occurrence of BPs when such a process considers the contraction of the skyrmion's core [18]. A similar event occurs when switching the polarity of a vortex core hosted in a magnetic nanodot [21]. Thus, a BP can be identified as a three-dimensional (3D) magnetic soliton with a vanishing magnetization field at its center which possesses exotic topological properties. Specifically, in a closed surface around its center, the direction of the magnetization field covers the whole solid angle an integer number of times, i.e., if the norm of the magnetization field is preserved, it translates into topological protection. In other words, the two-dimensional topological charge is an integer number. In contrast, its 3D topological charge, or the Hopf number, was only recently fully computed, showing that it can take non-integer values due to the contribution of the magnetostatic energy [22].

From an experimental point of view, it has recently been possible to image 3D magnetic configurations by using magnetic tomography based on electron holography or X-ray magnetic circular dichroism [23]. As stated above, this class of three-dimensional magnetic solitons can be found in cylindrical nanostructures such as nanowires or nanodots [12]. There is currently vast experience in manufacturing magnetic nanowires, nanodisks and nanodots through distinct experimental techniques. The proper control on the geometrical parameters of magnetic nanowires allows even to control the diameter of such structures, synthesizing the so-called diameter-modulated nanowires [24–33]. The main virtue of this kind of nanostructures, is that the region with a pronounced modulation in the diameter provides a pinning

* Corresponding author.
E-mail address: nicolas.vidal@ufrontera.cl (N. Vidal-Silva).

https://doi.org/10.1016/j.rinp.2022.105530
Received 14 March 2022; Received in revised form 6 April 2022; Accepted 18 April 2022
Available online 21 April 2022

potential, which depends on the geometry and the position of the modulation [34].

If two different magnetic orientations coexist within a nanowire, a reversion process can be triggered by different mechanisms (spontaneous, magnetic field, electrical current, or temperature gradient). The propagation of the domain wall could be stopped or stabilized at the modulation depending on the balance of geometry and intervening interactions. This feature opens the possibility of stabilizing a particular domain wall in the modulation. In specific, we are interested in stabilizing a Vortex Domain Wall (VDW) in a diameter-modulated nanowire because the central part of such structures configure itself as a BP. That is the reason this kind of domain wall is sometimes called Bloch Point Domain Wall (BPDW).

The stabilization of BPs in terms of the geometrical parameters is a topic that has recently gained the attention of many researchers. Indeed, some of us have searched for some signatures about it in a recent work related to the possibility of storing information in diameter-modulated nanowires [35]. Therefore, the conditions to confine BPs in a controlled way is an issue that, although still not completely explored, there are certain insights on how to achieve it. A more exotic and intriguing scenario occurs when a confined BP is excited with a magnetic pulse and its absorption spectrum is studied. This is an unexplored scenario where its importance relies on how the different spin-wave modes are excited around a confined BP. Considering the exotic and well-known dynamical properties of other topological solitons as skyrmions or vortices [36,37], the dynamical response that a BP would have when applying a magnetic pulse lacks at present a detailed analysis.

The dynamical response of cylindrical nanowires has been well studied in the past [38,39]. A geometrically homogeneous and uniformly magnetized nanowire has been well characterized when excited with a microwave field. The low energy excitations correspond to the edge modes localized at the end of the nanowire, while higher energy spin-wave modes localized at the bulk of the nanostructure are called the bulk modes. Recently, it was shown that incorporating a geometrical modulation on the diameter allows for adding new transitions resonance modes, which behave like transitions peaks between the edge and bulk modes [40].

In this work, by using micromagnetic simulations, we take advantage of the possibility of confining a BP within a diameter-modulated magnetic nanowire to stabilize and then study the dynamical response of the system when subjected to a magnetic pulse applied perpendicular to it. We aim to find and uncovering the different resonant modes that a magnetic nanowire can display in the presence of a confined BP in a geometric modulation. The focus of the present study is to analyze how the resonance modes of a modulated nanowire hosting a BP change when we alter the external conditions. This can be achieved by moving the position of the modulation or when we subject the system to external magnetic fields (for now, we consider fields parallel to the nanowire axis only).

This paper is organized as follows: the next section describes the Micromagnetic simulations; the third section is dedicated to results and discussions, where we have separated the dynamical response in two, first as a function of the position of the modulation and then as a function of the external magnetic field. The last section corresponds to the conclusions. Additionally, we prepared a separate file with Supplementary Information to provide for a wider basis for deeper discussions.

Micromagnetic simulations

For our micromagnetic simulations, we have used the free licensed software Mumax3 [41] by discretizing the space into cubic cells of $2 \times 2 \times 2$ nm^3. The nanowire is characterized by a length L, diameter d, and the modulation has the shape of a nanodisk with height W, diameter D and is located at a position z, that we consider variable, and measured from the basis of the nanowire ($z = 0$), as depicted in Fig. 1.

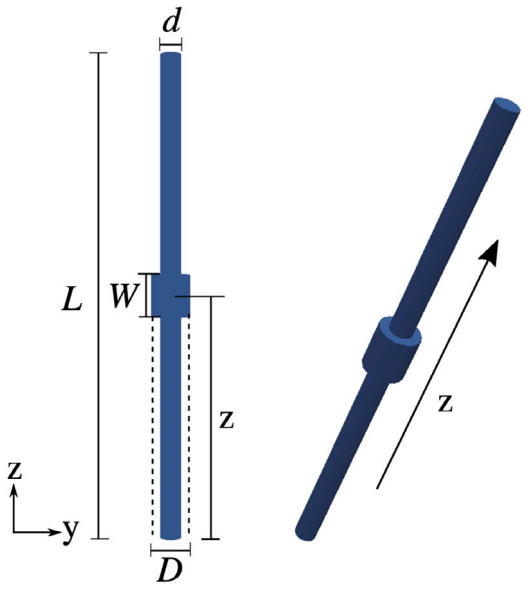

Fig. 1. Schematic representation of the system studied.

The stabilization of the BP depends on the magnetic and the geometrical parameters chosen. For such a purpose, we have fixed L = 1100 nm, d = 50 nm, W = 100 nm, and D = 90 nm, and the nanowire is considered being composed by $Ni_{80}Fe_{20}$ (Py), a magnetic material whose magnetocrystalline anisotropy can be neglected [42] in such a way that only the exchange and dipole–dipole interactions are the responsible for the stabilized (meta)stable states. To get a BP domain wall as a metastable state, we artificially imposed a tail-to-tail magnetic configuration as initial state and then leave the system reach a local minimum which results in a VDW or, more specifically, a BPDW as shown in the Fig. 2. Concretely, we numerically solve during 5 ns the Landau–Lifshitz–Gilbert (LLG) equation:

$$\dot{\mathbf{m}} = -\gamma \mathbf{m} \times \mathbf{H}_{\text{eff}} + \alpha \mathbf{m} \times \dot{\mathbf{m}}, \tag{1}$$

where γ is the gyromagnetic ratio, $\alpha = 0.5$ the phenomenological Gilbert damping, and $\mathbf{H}_{\text{eff}}$ is the effective field defined as $\mu_0 \mathbf{H}_{\text{eff}} = -\delta E_m[\mathbf{M}]/\delta \mathbf{M}$, being $\delta/\delta \mathbf{M}$ the variational derivative with respect to the magnetization $\mathbf{M}$; and the magnetic energy E_m is defined as

$$E_m[\mathbf{m}] = \int_V \mathrm{d}V \left[A \sum_{i=x,y,z} (\nabla m_i)^2 - \frac{\mu_0}{2} \mathbf{M} \cdot \mathbf{H}_d - \mathbf{M} \cdot \mathbf{B} \right], \tag{2}$$

that corresponds to the exchange interaction with stiffness constant A, the dipolar energy expressed in terms of the magnetostatic field $\mathbf{H}_d$, and the last term corresponds to the Zeeman interaction, respectively; $\mathbf{m} = \mathbf{M}/M_s$ stands for the normalized magnetization, M_s is the saturation magnetization, μ_0 the vacuum susceptibility, and $\mathbf{B}$ is an external magnetic field that might consider static or dynamical components. For all our calculations, the magnetic parameters we used are the corresponding to the Py [43]: $A = 13 \times 10^{-12}$ J/m and $M_s = 800 \times 10^3$ A/m. As a first state, in the procedure of obtaining the BPDW as a metastable state, we have considered absence of any external magnetic field. As we mentioned earlier, Fig. 2 shows a schematic of the initial and final state of our micromagnetic simulations. Although the reached state does not correspond to the ground state of the system, it is a metastable state comprising a vortex domain wall with a Bloch Point singularity in its center (see Fig. 2), which becomes the starting point for studying the dynamical response [44].

A possible way to inscribe a polarization as the one defined in Fig. 2 is to make use of the different shape anisotropy presented by

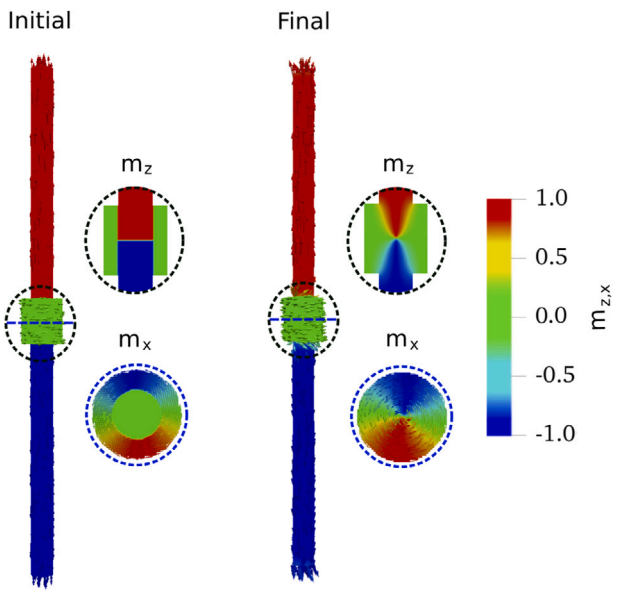

Fig. 2. Left panel: initial state for the micromagnetic simulations. Right panel: Final state after solving the LLG equation during 5 ns. The circled images correspond to the z- and x- component of the magnetization field when cuts along yz and xy planes are made, respectively.

rods and disks due to their distinct aspect ratios [45,46]. Thus, long wires (segments of the device) will naturally develop axial anisotropy; external magnetic fields can induce the needed polarity along the axis. On the other hand, disks (modulation of the device) tend to develop transverse or vortex domains in the planes perpendicular to the cylindrical axis. So, what is needed is to locate the device near the appropriate external magnetic fields to induce polarities that their geometrical components naturally sustain. To achieve the head-to-head configuration proposed in Fig. 2 the segments can be located between the north poles of strong magnets or electromagnets. At the same time, on the central plane of the modulation and surrounding it, several curved magnets (like the usual horseshoe magnets) can be displayed to produce curling magnetization fields with the desired chirality to induce the vortex within the modulation. The resulting configuration will naturally minimize energy to reach a metastable state.

Once the metastable state is stabilized, the next step is to excite such a configuration with a microwave magnetic pulse of the form $\mathbf{h}(t) = 1.0 \times \exp\left(-10^9 t\right) \hat{\mathbf{y}}$ kA/m [47–52]. The amplitude of this pulse must be small enough to keep the system in the linear response regime [49,53]. The dynamical response is also obtained by numerically solving the LLG equation but now using $\alpha = 0.015$ (value that is lower than 0.2 commonly used for a dynamic study [48,54,55]) and the magnetic energy E_m now considers the additional contribution to the Zeeman term coming from the application of the dynamical microwave field. The temporal evolution of the magnetization under the action of the exciting field is collected for 20 ns recording the magnetization configuration at uniform time intervals of 5 ps allowing a spectral resolution of 0.05 GHz [56,57].

The analysis of the recorded data continues now in the following way: the small exciting magnetic field $h(t)$ and the magnetization distribution $M(\mathbf{r}, t)$ are transformed to the frequency domain $[h(\omega), M(\omega)]$ using the Fast Fourier Transform (FFT) method. The dynamic susceptibility, which corresponds to the imaginary part of the magnetic susceptibility, is calculated by dividing the Fourier transform of the response $M(\omega)$ by the Fourier transform of the excitation $h(\omega)$. Finally, in order to confirm the origin of the resonant peaks, we can reconstruct the spatial profiles of the resonant modes [58,59] by calculating the temporal Fourier image for each site as $\tilde{m}(r_{ijk}, f_n) = \mathrm{DFT}_t\left(m(r_{ijk}, t)\right)$, where DFT_t is the Discrete-time Fourier Transform, the subscript ijk corresponds to the spatial coordinates x, y, z of each cell, and the subscript n refers to the position of the frequency in the power spectra. These images are essentially the profiles of the magnetization for any frequency.

Results and discussions

Dynamical response as a function of the position of the modulation

Our dynamical study begins by analyzing the zero-field case (i.e., only the microwave magnetic pulse contributes to the Zeeman term in the effective field), and we focus on the dependence that the spin-wave modes have on the position at which the modulation is located. This section then intends to elucidate the role that the modulation and its position have on the dynamical response of the confined BP. In other words, here we ask about how the geometry of the system affects the dynamical response of it. A related article previously published addressed a similar system but with a different magnetic configuration as a metastable state in the modulation [50]. Here, the presence of the BP completely changes the condition of the problem.

We start by considering the modulation in the half of the nanowire ($z = 550$ nm) and then we displace the modulation towards the top end of the nanowire in steps of 10 nm. Fig. 3 shows the frequency of the resonance modes as a function of the position at which the modulation is located. In Fig. 3(a) we show a tracing of the resonance modes, and the colored circles corresponds to three selected positions of the modulation for each resonance mode, whose origin is represented by the spatial distribution of the spin-wave modes in Fig. 3(b). From Fig. 3(a) we can identify 5 modes with variable amplitude, as evidenced by the color bar varying from the most intense modes (white) to the less ones (black). It has been previously established that in cylindrical nanowires with geometrical modulations, the lowest energy mode corresponds to the edge mode; the next higher frequency mode is due to the modulation itself; high energy modes can be recognized as bulk modes [48]. These features are mainly attributed to the competition between the exchange interaction and the magnetostatic energy induced by the modulation [50,60], whose dynamical response is altered due to the presence of a BP within modulation. The zone affected by the mode presents magnetization polarizations as presented by the color variations in Fig. 3(b). The corresponding frequency is given in Fig. 3(a).

Let us firstly focus on the case $z = 550$ nm. In this case, the lowest energy mode for this choice of parameters is still the edge mode. However, the next two modes (modes 2 and 3) are exclusively activated due to the presence of the BP singularity and its dynamics. Indeed, the center of the BP has the maximum spin amplitude (red color), while the rest of the nanostructure is not excited, as depicted in Fig. 3(b) (see the first row for modes 2 and 3). Therefore, the presence of the BP is responsible for activating modes 2 and 3, and the difference between them lies in how the BP environment is excited. Modes 4 and 5 correspond to the so-called bulk modes, where the entire nanowire is excited. Note that mode 5 has the largest amplitude because, in this case, there is a major portion of magnetic material excited with high spin amplitudes.

Next, we examine the system when the modulation moves towards the top end of the nanowire. Let us firstly focus on the positions $z < 900$ nm. As we can see from Fig. 3, modes 1, 2, and 3 are almost unaltered in the entire range considered. However, a different behavior occurs for $z \geq 900$ nm, as will be discussed below. The reason why these modes remain constant for a large range of the position z can be understood in terms of the nature of the modes: Mode 1 corresponds to edge mode localized at the end of the nanowire, so it is only affected by the stray field produced by the modulation when localized near the ends. A similar behavior occurs for modes 2 and 3, which are activated due to the presence of the BP singularity. Again, once the interaction

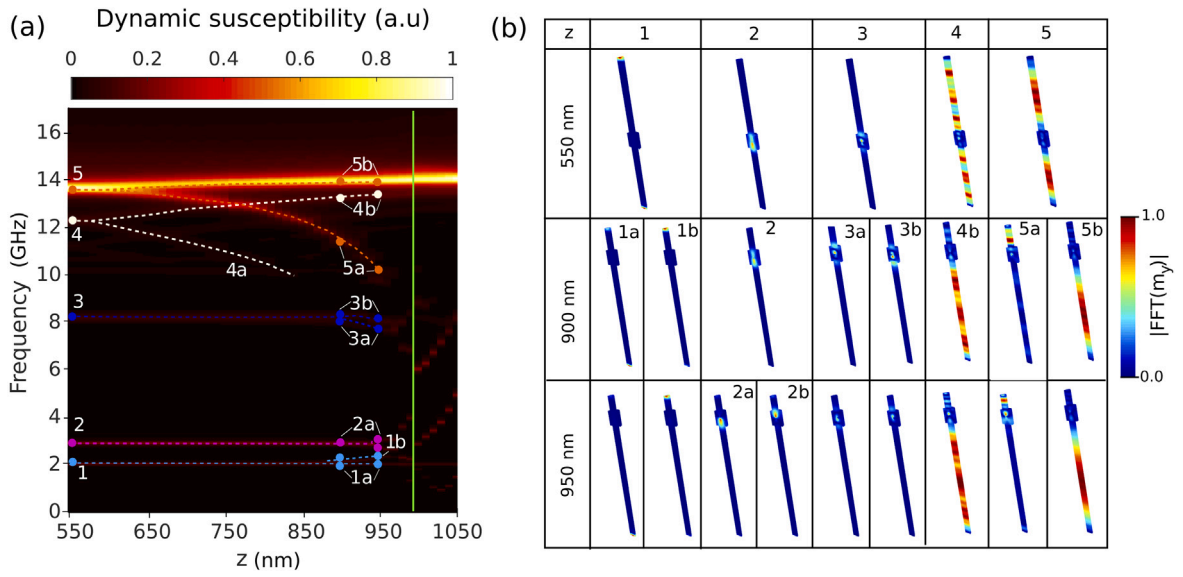

Fig. 3. (a) Frequency of the resonance modes as a function of the position at which the modulation is located. The lines cyan, purple, blue, white, and orange correspond to the modes 1, 2, 3, 4, and 5, respectively. The small solid circles denote the corresponding spin distribution shown in the right panel. The vertical green line is included to depict the position of the modulation at which the system no longer stabilizes the BP and ultimately relaxes into the homogeneous state. The color bar represents the amplitude of the y-component of the absorption spectrum. (b) Spatial distribution of the selected resonance modes depicted with small solid circles in the left panel. Here, in the vertical color bar located at the right, the amplitude varies from maximum (red color) to minimum (blue color). (For interpretation of the references to color in this figure legend, the reader is referred to the web version of this article.)

between the ends of the nanowire with the BP singularity becomes slightly appreciable, then the resonance modes change their behavior, as depicted in Fig. 3(a).

Modes 4 and 5 are affected when moving the modulation towards the end of the nanowire. As shown in this figure, each of these modes split into two new modes, modes 4a (5a) and 4b (5b). This behavior can also be understood by the nature of the modes. In fact, since these modes correspond to bulk ones, they are characterized by the spin excitation of the entire nanostructure; therefore, it is natural to expect that changes in the geometry provoke changes in the resonance modes. We argue that the emergence of modes 4a (5a) and 4b (5b) is because of the modulation that makes the system behave like two separated nanowires. Thus, the bulk modes separate according to the two different sections of the nanowire separated by the modulation. Note that mode 4a vanishes for $z \geq 800$ nm because this mode corresponds to the spin excitation of a smaller section of the nanowire so that, when approximating to the end, there is not enough volume magnetic to be excited. The same reason applies for mode 5a, which does not disappear, but its resonance frequency decreases considerably while the position z increases, as suggested in Fig. 3(b) in the second row.

The region $z \geq 900$ nm is more interesting, where the three lowest energy modes present splitting. First, mode 1 splits into modes 1a and 1b. As seen from Fig. 1(b) in the middle and bottom row, modes 1a and 1b correspond to the spin excitation localized in the bottom end of the nanowire (mode 1a) and the top end (mode 1b). Such splitting relies on the fact that the system behaves like two different nanowires separated by the modulation. Then, each of these nanowires has its own edge mode, corresponding to modes 1a and 1b. A similar behavior can be found when the modulation is at $z = 950$ nm. In both cases, the emergent modes correspond to edge modes.

The splitting of modes 2 and 3 occurs for a completely different reason. Recall that these modes are activated by the BP stored within the modulation. Note that mode 2 holds at $z = 900$ nm, and modes 2a and 2b only appear at $z = 950$ nm. As evidenced in the bottom row in Fig. 3(a), these emergent modes correspond to the BP excitation in the upper and lower half of the modulation, respectively. Since for $z \geq 950$ the system cannot stabilize a BP within the modulation, we conclude that the splitting modes appear as a feature of the system when it is near ejecting the BP from the modulation. This behavior can also be identified for mode 3; however, in this case, this mode already split into modes 3a and 3b at $z = 900$ nm. For $z = 900$ nm, the demagnetizing field produced by the upper end is noticeable enough to make the BP unstable within the modulation. Again, once the modulation reaches $z = 950$ nm, the stability of the BP weakens, and for even larger z, the pseudo-homogeneous state is favored. A further analysis of the BP stability is developed in Supplementary Information. Finally, modes 4 and 5 (bulk modes) split at a modulation position close to half of the nanowire. In these cases, Fig. 3(b) shows that this splitting agrees with the above hypothesis that the nanowire behaves like two independent nanowires. In fact, modes 5a and 5b (also 4a and 4b) correspond to the separated excitation of the upper and lower segments of the nanowire.

Dynamical response as a function of the external magnetic field

In this section, we focus on the effects that the application of an external magnetic field has on the spin-wave modes of the system when keeping the position of the modulation fixed. Therefore, the primary purpose of this section is to clarify how the internal magnetic structure (which changes because of the application of the external magnetic field) of the BP affects the spin-wave modes of the system while leaving the geometry unchanged.

The procedure we follow here differs slightly from the past section. We consider the same geometry, but the modulation now remains unchanged at half of the nanowire ($z = 550$ nm). Next, we apply a constant external magnetic field (bias field) along the $(-z)$–direction and let the system relaxes until it reaches a metastable state. This state is considered as the initial state, which is ultimately perturbed by applying a small magnetic pulse along the perpendicular axis to the nanowire. The results regarding the dynamic properties are collected in the same way as the past section, and they can be summarized in Fig. 4, where we show the frequency of the resonance modes as a function of the external magnetic field and the spatial distribution of the spin-wave modes at selected resonance frequencies (depicted with small circles in Fig. 4(a)).

Fig. 4(a) shows modes 1 through 5, and their dependence on the magnitude of the external magnetic field along the axial direction. We

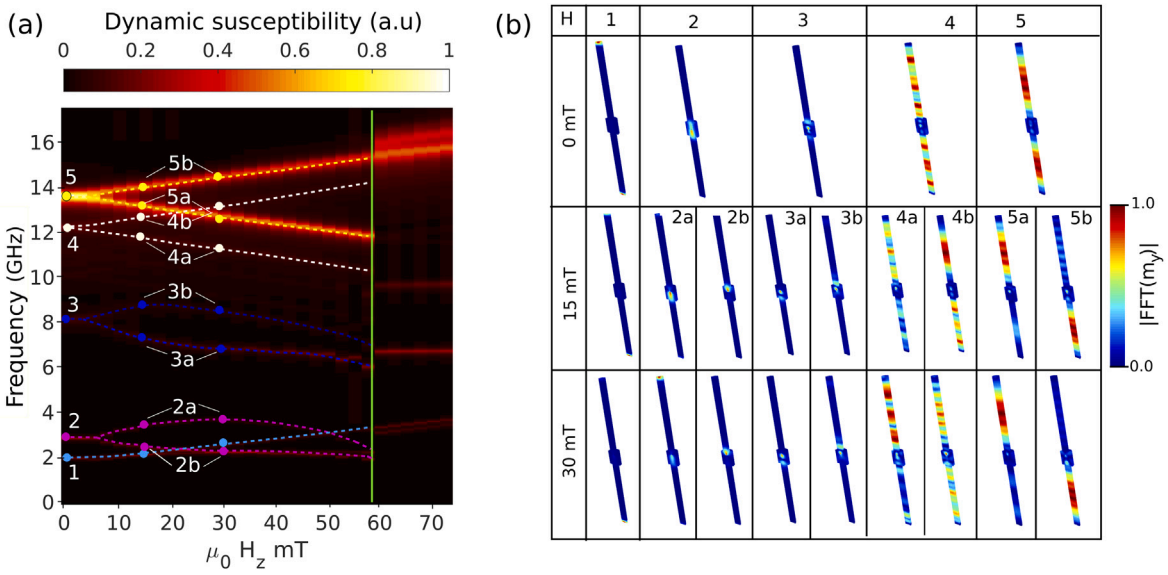

Fig. 4. The response of the system to the external excitation is depicted in this illustration. (a) This panel gives the frequency dependence on the intensity of the applied magnetic field. (b) This panel presents the modes for 3 values of the external field by means of a color code given to the extreme right: red corresponds to large precession amplitude as opposed to blue which means zero amplitude. The labels for the modes are given at zero field to the left of panel (a), as 1, 2, 3, 4, and 5, using different colors. The splittings are clearly appreciated as the field increases and the corresponding new frequencies are labeled by adding a or b to the original mode label. The solid circles refer to the values of the field used in the panel (b). As the field increases to the right it eventually reaches a critical value (illustrated by the vertical green line at 59 mT) at which the BP relaxes into the homogeneous state. (For interpretation of the references to color in this figure legend, the reader is referred to the web version of this article.)

can identify several aspects with similar behavior as those discussed in relation to Fig. 3. For instance, we have also depicted with a green line the limit scenario when the system is no longer capable of stabilizing the BP within the modulation. This occurs for a field $\sim$ 59 mT. For fields higher than it, the system relaxes into a homogeneous state. We start by considering the edge mode, which corresponds to the excitation of spins at the end of the nanowire. As seen from Fig. 4(a), this mode has monotonic increasing with the magnetic field. Note that, unlike the previous case, mode 1 does not split. This can be explained in terms of the effect that the magnetic field has on the magnetic configuration of the nanowire. In fact, as long the magnetic field increases, the system aligns the spins in such a direction so that the microwave field can no longer separately activate the two ends of the nanowire. Instead, as presented in Fig. 4(b), mode 1 is characterized by the excitation of both ends at 0 and 15 mT. Still, when increasing the field to 30 mT, only the bottom end is excited, which explains the absence of a splitting mode.

Modes 2 and 3, are split when increasing the magnetic field. Specifically, mode 2 splits into modes 2a and 2b at $\sim$ 15 mT and mode 3 splits into modes 3a and 3b at $\sim$ 3 mT, as seen in Fig. 4(a). We can see from Fig. 4(b) that mode 2 at 0 mT corresponds to the BP excitation. However, at 15 and 30 mT, modes 2a and 2b correspond to the BP excitation in the upper and lower half of the modulation. Note that this behavior is analog to moving the modulation along the nanowire axis. For mode 3, and the corresponding modes 3a and 3b, the effect of applying a magnetic field is pretty like the one reported in the previous section. Indeed, the application of a magnetic field promotes the separated excitation of the two distinct regions within the modulation. Moreover, the bulk modes 4 and 5 split into modes 4a (5a) and 4b (5b) if the magnetic field is nonzero. From Fig. 4(b) we can see that mode 4 at zero field is characterized by the spin excitation of the entire nanowire excepting the modulation zone, just like if we would consider two separated nanowires. Furthermore, the amplitude of the excitation is variable along the two sections. Once the magnetic field increases, the system holds exciting the same regions as at zero field, but now the amplitude varies differently in the two sections, which explains the presence of modes 4a and 4b. Finally, the highest frequency mode, mode 5, splits into modes 5a and 5b at low magnetic fields. Note that mode 5 at zero field corresponds to a higher spin excitation of the two separated (by the modulation) sections of the nanowire. However, when increasing the magnetic field, these sections are separately excited. Indeed, at 15 mT the modes 5a and 5b correspond to the excitation of the upper and bottom section, respectively. The same happens at 30 mT, where the excited regions are notoriously more pronounced.

Conclusions

We have performed a detailed analysis of the dynamic properties of a diameter-modulated nanowire with a BP singularity hosted within the geometrical modulation. We have considered two aspects capable of modifying the dynamic properties: the position of the modulation and the strength of an external magnetic field. In both cases, we identified five modes: mode 1 corresponding to the edge mode, while modes 2 and 3 emerge due to the presence of the BP. Modes 4 and 5 are the bulk modes. When changing the modulation position, we found that the three lowest modes are almost unaltered until the modulation reaches a critical region at which the stray field generated by the end of the nanowire is strong enough to interact with the modulation. Interestingly, the BP modes (modes 2 and 3) split into two new modes, respectively. We attribute this behavior to the system being near to revert the magnetization, and therefore the BP within the modulation becomes unstable, allowing then to excite two different modes.

A similar behavior is found when applying an external magnetic field. Here, we also reported five modes with the same features as the above case. Again, the BP modes split into two new modes when increasing the magnetic field. The origin of these modes is the same as when changing the modulation position. Therefore, we also attributed this splitting to that the system tends to revert its magnetization. In fact, in the presence of certain magnetic fields, the BP is always being pushed out of the modulation, which agrees with the case when the modulation is near the end of the nanowire, where the effect of the stray field generated by the end on the modulation is essentially to eject the BP from the modulation. Thus, we have explored a system capable of hosting a BP singularity as a metastable state and whose dynamic properties strongly depend on the geometrical parameters and the application of an external magnetic field. The main contribution of

our work relies on the fact that we characterized a system that is excited when the BP localizes within the modulation. In this sense, the behavior of the system might be useful in recognizing the presence or absence of a BP singularity by only exploring the splitting of certain modes. Specifically, we showed that the first two *optical* modes correspond to the BP modes, so that, when applying a magnetic field, these modes will split into two new modes. Similarly, by locating the modulation near the end of the nanowire, our results predict the splitting of the first two optical modes, which is an unequivocal signature of the presence of a BP. It is important to point out that the behavior obtained in our results could have variations according to the choice of the magnetic and geometrical parameters. Therefore, to extract analytical and general results from them is an issue that is out of the scope of the present study, and we leave it for future works.

CRediT authorship contribution statement

Guidobeth Sáez: Conceptualization, Software, Visualization, Formal analysis. **Eduardo Saavedra:** Conceptualization, Software, Visualization, Formal analysis. **Nicolás Vidal-Silva:** Conceptualization, Methodology, Formal analysis, Writing – original draft. **Juan Escrig:** Conceptualization, Resources, Formal analysis, Writing – original draft. **Eugenio E. Vogel:** Conceptualization, Resources, Formal analysis, Writing – original draft.

Declaration of competing interest

The authors declare that they have no known competing financial interests or personal relationships that could have appeared to influence the work reported in this paper.

Acknowledgments

This work was partially supported by Fondecyt, Chile (grant numbers 11220046, 1190036, and 1200302), Basal Project Cedenna, Chile (ANID grant number AFB180001) and ANID through its program ANID-Subdirección de Capital Humano/Doctorado, Chile Nacional/2022-21222167.

Supplementary data

Supplementary material related to this article can be found online at https://doi.org/10.1016/j.rinp.2022.105530. There, the stability of the Bloch Point singularity as the starting point for the dynamical study is studied as a function of the external magnetic field and the modulation position.

References

[1] Kou X, Fan X, Dumas RK, Lu Q, Zhang Y, Zhu H, et al. Adv Mater 2011;23(11):1393–7.
[2] Darques M, De la Torre Medina J, Piraux L, Cagnon L, Huynen I. Nanotechnology 2010;21(14):145208.
[3] Parsa N, Gasper MR, Karempudi VSP, Toonen RC. 2018 IEEE 13th nanotechnology materials and devices conference. IEEE; 2018, p. 1–4.
[4] Sharma M, Kuanr BK, Sharma M, Basu A. J Appl Phys 2014;115(17):17A518.
[5] Zhou W, Um J, Stadler B, Franklin R. 2018 IEEE radio and wireless symposium. IEEE; 2018, p. 240–2.
[6] Arzuza L, López-Ruiz R, Salazar-Aravena D, Knobel M, Beron F, Pirota KR. J Magn Magn Mater 2017;432:309–17.
[7] Raviolo S, Pereira A, Jaimes DMA, Escrig J, Bajales N. J Magn Magn Mater 2020;499:166240.
[8] Zhang G-F, Li Z-X, Wang X-G, Nie Y-Z, Guo G-H. Chin Phys B 2015;24(9):097503. http://dx.doi.org/10.1088/1674-1056/24/9/097503.
[9] Barman A, Mondal S, Sahoo S, De A. J Appl Phys 2020;128(17):170901. http://dx.doi.org/10.1063/5.0023993.
[10] Barman A, Gubbiotti G, Ladak S, Adeyeye AO, Krawczyk M, Gräfe J, et al. J Phys: Condens Matter 2021;33(41):413001.
[11] Tejo F, Saavedra E, Denardin JC, Escrig J. Appl Phys Lett 2020;117(15):152401. http://dx.doi.org/10.1063/5.0023613.
[12] Shevchenko A, Barabash MY. Appl Nanosci 2022;1–5.
[13] Elías RG, Verga A. Eur Phys J B 2011;82(2):159–66.
[14] Pylypovskyi OV, Sheka DD, Gaididei Y. Phys Rev B 2012;85(22):224401.
[15] Wartelle A, Trapp B, Staño M, Thirion C, Bochmann S, Bachmann J, et al. Phys Rev B 2019;99(2):024433.
[16] Li Y, Pierobon L, Charilaou M, Braun H-B, Walet NR, Löffler JF, et al. Phys Rev Res 2020;2(3):033006.
[17] Müller GP, Rybakov FN, Jónsson H, Blügel S, Kiselev NS. Phys Rev B 2020;101(18):184405.
[18] Birch MT, Cortés-Ortuño D, Khanh ND, Seki S, Štefančič A, Balakrishnan G, et al. Commun Phys 2021;4(1):1–9.
[19] Charilaou M, Braun H-B, Löffler JF. Phys Rev Lett 2018;121(9):097202.
[20] Zou J, Zhang S, Tserkovnyak Y. Phys Rev Lett 2020;125(26):267201.
[21] Pylypovskyi OV, Sheka DD, Kravchuk VP, Gaididei Y. Low Temp Phys 2015;41(5):361–74.
[22] Tejo F, Heredero RH, Chubykalo-Fesenko O, Guslienko K. Sci Rep 2021;11(1):1–9.
[23] Chauleau J-Y, Legrand W, Reyren N, Maccariello D, Collin S, Popescu H, et al. Phys Rev Lett 2018;120(3):037202.
[24] Salem MS, Tejo F, Zierold R, Sergelius P, Moreno JMM, Goerlitz D, et al. Nanotechnology 2018;29(6):065602.
[25] Fernandez-Roldan JA, Del Real RP, Bran C, Vazquez M, Chubykalo-Fesenko O. Nanoscale 2018;10(13):5923–7.
[26] Bran C, Fernandez-Roldan JA, Del Real RP, Asenjo A, Chubykalo-Fesenko O, Vazquez M. Nanomaterials 2021;11(3):600.
[27] Nasirpouri F, Peighambari-Sattari S-M, Bran C, Palmero EM, Berganza Eguiarte E, Vazquez M, et al. Sci Rep 2019;9(1):1–11.
[28] Méndez M, Vega V, González S, Caballero-Flores R, García J, Prida VM. Nanomaterials 2018;8(8):595.
[29] Moreno JA, Bran C, Vazquez M, Kosel J. IEEE Trans Magn 2021;57(4):1–17.
[30] Bran C, Fernandez-Roldan JA, P. Del Real R, Asenjo A, Chen Y-S, Zhang J, et al. ACS Nano 2020;14(10):12819–27.
[31] Fernández-Roldán JA, De Riz A, Trapp B, Thirion C, Vazquez M, Toussaint J-C, et al. Sci Rep 2019;9(1):1–12.
[32] Arzuza LC, Vega V, Prida VM, Moura KO, Pirota KR, Béron F. Nanomaterials 2021;11(12):3403.
[33] García J, Fernández-Roldán JA, González R, Méndez M, Bran C, Vega V, et al. Nanomaterials 2021;11(11):3077.
[34] Sáez G, Cisternas E, Diaz P, Vogel EE, Burr JP, Saavedra E, et al. J Magn Magn Mater 2020;512:167045.
[35] Sáez G, Díaz P, Cisternas E, Vogel EE, Escrig J. 2021;11(1). http://dx.doi.org/10.1038/s41598-021-00165-1.
[36] Tejo F, Saavedra E, Denardin J, Escrig J. Appl Phys Lett 2020;117(15):152401.
[37] Saavedra E, Palma J, Escrig J. J Magn Magn Mater 2022;541:168493.
[38] Dao N, Donahue M, Dumitru I, Spinu L, Whittenburg S, Lodder J. Nanotechnology 2004;15(10):S634.
[39] Liu R, Wang J, Liu Q, Wang H, Jiang C. J Appl Phys 2008;103(1):013910.
[40] Saavedra E, Saez G, Díaz P, Cisternas E, Vogel EE, Escrig J. AIP Adv 2019;9(6):065007.
[41] Vansteenkiste A, Leliaert J, Dvornik M, Helsen M, Garcia-Sanchez F, Van Waeyenberge B. AIP Adv 2014;4(10):107133. http://dx.doi.org/10.1063/1.4899186.
[42] Kateb M, Gudmundsson JT, Ingvarsson S. AIP Adv 2019;9(3):035308. http://dx.doi.org/10.1063/1.5088602.
[43] Gérardin O, Youssef JB, Le Gall H, Vukadinovic N, Jacquart PM, Donahue MJ. J Appl Phys 2000;88(10):5899–903. http://dx.doi.org/10.1063/1.1320011.
[44] Baker A, Beg M, Ashton G, Albert M, Chernyshenko D, Wang W, et al. J Magn Magn Mater 2017;421:428–39. http://dx.doi.org/10.1016/j.jmmm.2016.08.009.
[45] Landeros P, Escrig J, Altbir D, Laroze D, e Castro Jd, Vargas P. Phys Rev B 2005;71(9):094435.
[46] Moreno R, Carvalho-Santos V, Altbir D, Chubykalo-Fesenko O. J Magn Magn Mater 2022;542:168495.
[47] Wang J, Zhang B, Liu Q, Ren Y, Liu R. J Appl Phys 2009;105(8):083908. http://dx.doi.org/10.1063/1.3108537.
[48] Dao N, Donahue MJ, Dumitru I, Spinu L, Whittenburg SL, Lodder JC. Nanotechnology 2004;15(10):S634–8. http://dx.doi.org/10.1088/0957-4484/15/10/022.
[49] Liu R, Wang J, Liu Q, Wang H, Jiang C. J Appl Phys 2008;103(1):013910. http://dx.doi.org/10.1063/1.2829817.
[50] Saavedra E, Saez G, Díaz P, Cisternas E, Vogel EE, Escrig J. AIP Adv 2019;9(6):065007. http://dx.doi.org/10.1063/1.5091813.
[51] Saavedra E, Palma J, Escrig J. J Magn Magn Mater 2022;541:168493. http://dx.doi.org/10.1016/j.jmmm.2021.168493.
[52] Saavedra E, Vidal-Silva N, Escrig J. Results Phys 2021;31:104874. http://dx.doi.org/10.1016/j.rinp.2021.104874.

[53] Wagner K, Körber L, Stienen S, Lindner J, Farle M, Kákay A. IEEE Magn Lett 2021;12:1–5. http://dx.doi.org/10.1109/LMAG.2021.3055447.
[54] Wang Q, Jin L, Tang X, Bai F, Zhang H, Zhong Z. IEEE Trans Magn 2012;48(11):3246–9. http://dx.doi.org/10.1109/TMAG.2012.2197674.
[55] Russek SE, Kaka S, Donahue MJ. J Appl Phys 2000;87(9):7070–2. http://dx.doi.org/10.1063/1.372934.
[56] Kim J-V, Garcia-Sanchez F, Sampaio J, Moreau-Luchaire C, Cros V, Fert A. Phys Rev B 2014;90:064410. http://dx.doi.org/10.1103/PhysRevB.90.064410.
[57] Mehmood N, Wang J, Zhang C, Zeng Z, Wang J, Liu Q. J Magn Magn Mater 2022;545:168775. http://dx.doi.org/10.1016/j.jmmm.2021.168775.
[58] McMichael RD, Stiles MD. J Appl Phys 2005;97(10):10J901. http://dx.doi.org/10.1063/1.1852191.
[59] Kumar D, Dmytriiev O, Ponraj S, Barman A. J Phys D: Appl Phys 2011;45(1):015001. http://dx.doi.org/10.1088/0022-3727/45/1/015001.
[60] Xiong LL, Kostylev M, Adeyeye AO. Phys Rev B 2017;95:224426. http://dx.doi.org/10.1103/PhysRevB.95.224426.